Comparing Analytical Approximation Methods with Numerical Results for Nonlinear Systems

A.J. Elliott, A. Cammarano, S.A. Neild

Abstract

Modelling the dynamics of nonlinear systems poses a much more challenging problem than for their linear counterparts; as such, analytical solutions are rarely achievable and numerical or analytical approximations are often necessary to understand the system's behaviour. While numerical techniques are undoubtedly accurate, it is possible to gain a greater understanding of the processes underpinning the workings of the dynamics.

Therefore, it is valuable to investigate the accuracy and practicality of the aforementioned analytical approximation techniques and compare the results with numerical which are known to be accurate. In this paper, the unforced, undamped dynamics (known as backbone curves) of a non-symmetric two-mass oscillator will be calculated using the second-order normals forms (SONF), harmonic balance, and multiple scales techniques. The results of these will then be compared to responses found using numerical continuation. Furthermore, the forced responses will be approximated using the SONF and harmonic balance techniques.

1 Introduction

Increasing demand for lightweight and flexible mechanical structures has led to a marked interest across the scientific community in the mathematical modelling of nonlinear dynamical systems. As with most complex structures, an exact analytical solution is not always achievable, nor is it particularly beneficial when approximations can be made to an extremely high level of accuracy (see, for example, [1]). While a full solution might not be available, a number of analytical approximations have been established; these allow the intricacies of the model to be maintained, while removing the unnecessary calculations of non-resonant terms. In this paper, three of these techniques will be considered: second-order normal forms (SONF) [1–3], harmonic balance [4], and multiple scales [5].

An increasingly common application of these techniques is to find the unforced, undamped responses, or *backbone curves*, of a system [3, 6]. Doing so allows the underlying behaviour of the system to be captured and, although they are not related to any particular forced case, they can still be used to indicate the occurrence of internal resonance within the structure [7]. Further, the techniques need only minor adaptations to give the forced, damped responses.

Numerical techniques for finding the system responses are well-established, though they are not as capable of revealing the system's behaviour as the aforementioned analytical approximations. To that end, this paper will compare the accuracy of these methods to the numerical results generated by the *AUTO-07p* numerical continuation software [8]. Initially, the backbone curves will be calculated using all three techniques. Following this, a selection of single- and mixed-mode forced and damped cases will be analysed using the SONF and harmonic balance techniques. The multiple scales method is not considered in this section, as the associated equations quickly became overly complex.

2 Analytical Approximations

2.1 Example System

The configuration under consideration in this paper is a non-symmetric, two-mass oscillator, with an underlying symmetric system of linear springs similar to that in [2, 3, 7]; a schematic is given in Figure 1. The

two masses in the system are identical and their displacements are denoted x_1 and x_2, respectively. The first mass is grounded by a nonlinear spring with force-deflection relationship $F = k_1(\Delta x) + \kappa_1(\Delta x)^3$ while the second is grounded by a linear spring with spring constant k_1. A second nonlinear spring, with force-deflection relationship $F = k_2(\Delta x) + \kappa_2(\Delta x)^3$, connects the two masses. Note that the underlying linear system, including damping, is symmetrical; two linear viscous dampers (with damping constants c_1) ground the masses and a further damper (with damping constant c_2) connects the two masses. The equations of motion for the system are as follows:

$$\mathbf{M}\ddot{\mathbf{x}} + \mathbf{K}\mathbf{x} + \mathbf{N}_{\mathbf{x}}(\mathbf{x}, \dot{\mathbf{x}}) = \mathbf{P}_{\mathbf{x}} \cos(\Omega \mathrm{t}) \tag{1}$$

where $\mathbf{x}$ is a vector of the displacements of the two masses, $\mathbf{M}$ and $\mathbf{K}$ are the mass and stiffness matrices, respectively, and $\mathbf{N}_{\mathbf{x}}(\mathbf{x}, \dot{\mathbf{x}})$ is a vector of the nonlinear and damping terms. $\mathbf{P}_x$ is a vector containing the physical forcing terms which, all of which are assumed to be at the same frequency, Ω.

Throughout this paper, the results will be displayed in linear modal coordinates; as such, the approximation techniques will be applied directly to the modal equations of motion. This is done through the use of the modeshape matrix, $\mathbf{\Phi}$, which is a matrix whose columns are the modeshapes of the linear modes. The transform takes the form $\mathbf{x} = \mathbf{\Phi}\mathbf{q}$ and results in the linear modal equations of motion

$$\ddot{\mathbf{q}} + \mathbf{\Lambda}\mathbf{q} + \mathbf{N}_{\mathbf{q}}(\mathbf{q}, \dot{\mathbf{q}}) = \mathbf{P} \cos(\Omega \mathrm{t}) \tag{2}$$

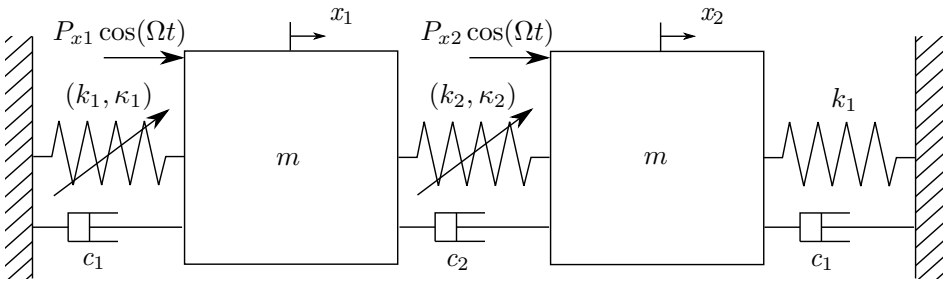

Figure 1: A schematic diagram of a two-degrees-of-freedom oscillator with a non-symmetric structure

2.2 Backbone Curves

Initially, the backbone curves are calculated using the analytical methods; this is due to the fact that the equations of motion are simplified by the fact that the forcing and damping terms are not considered. In the following calculations, the system is reduced to the unforced, undamped case by setting $c_1, c_2, P_1, P_2 = 0$ in the following calculations.

The equations of motion for the free vibration of the system can be written in the following form:

$$\mathbf{M}\ddot{\mathbf{x}} + \mathbf{K}\mathbf{x} + \mathbf{N}_{\mathbf{x}}(\mathbf{x}) = \mathbf{0} \tag{3}$$

where $\mathbf{N}_{\mathbf{x}}$ now contains only the nonlinear terms and is given by

$$\mathbf{N}_{\mathbf{x}}(\mathbf{x}) = \begin{pmatrix} \kappa_1 x_1^3 + \kappa_2 (x_1 - x_2)^3 \\ -\kappa_2 (x_1 - x_2)^3 \end{pmatrix} \tag{4}$$

In modal coordinates, the equations of motion are written as follows:

$$\ddot{\mathbf{q}} + \mathbf{\Lambda}\mathbf{q} + \mathbf{N}_{\mathbf{q}}(\mathbf{q}) = \mathbf{0} \tag{5}$$

For the system outlined in Figure 1, we have

$$\mathbf{\Phi} = \begin{pmatrix} 1 & 1 \\ 1 & -1 \end{pmatrix}, \ \mathbf{\Lambda} = \begin{pmatrix} \omega_{n1}^2 & 0 \\ 0 & \omega_{n2}^2 \end{pmatrix}, \ \mathbf{N}_{\mathbf{q}}(\mathbf{q}) = \frac{\kappa_1}{2\mathrm{m}} \begin{pmatrix} (q_1 + q_2)^3 \\ (q_1 + q_2)^3 + \alpha q_2^3 \end{pmatrix} \tag{6}$$

where $\alpha = 1 + 16\frac{\kappa_2}{\kappa_1}$ and ω_{ni} is the natural frequency of the i^{th} linear mode. The natural frequencies are assumed to be close and, hence, the response frequency of the system will be close to both of these, i.e. $\Omega \approx \omega_{n1} \approx \omega_{n2}$.

2.2.1 Harmonic Balance

The assumption of a sinusoidal response is again applied in this technique. Thus, the i^{th} mode will have a response of the form

$$q_i = A_i e^{+j\omega_r t} + \bar{A}_i e^{-j\omega_r t} \tag{7}$$

where $A_i = \frac{a_i}{2} e^{\alpha_i}$ contains information about the response amplitude (a_i) and phase (α_i).

Equation 5 can now be expanded in terms of these new definitions; these equations are again ungainly and are omitted. At this point, the "harmonic balance" can be applied. This entails equating the coefficient of one or more of the harmonics on either side of the equation. In this case, the first harmonic ($e^{+j\omega_r t}$) will be considered, resulting in the following equations, once the real and imaginary parts have been separated.

First Mode:

$$\begin{aligned}\frac{a_2}{2}(\omega_{n2}^2 - \omega_r^2 + \frac{3}{4}(3a_1^2\kappa_1 + a_2^2(\kappa 1 + 8\kappa 2)))\cos[\alpha_1 - \alpha_2] \\ + \frac{a1}{2}((\omega_{n1}^2 - \omega_r^2 + \frac{3}{4}((a_1^2 + 2a_2^2) + a_2^2\kappa_1\cos[2(\alpha_1 - \alpha_2)])) = 0\end{aligned} \tag{8}$$

$$-\frac{a_2}{2}(\omega_{n2}^2 - \omega_r^2 + \frac{3}{4}(a_1^2\kappa_1 + a_2^2(\kappa 1 + 8\kappa 2) + 2a_1a_2\kappa_1\cos[\alpha_1 - \alpha_2]))\sin[\alpha_1 - \alpha_2] = 0 \tag{9}$$

Second Mode:

$$\frac{a_2}{2}(\omega_r^2 - \omega_{n2}^2 - 6a_2^2\kappa_2) + \frac{a1}{2}(\omega_{n1}^2 - \omega_r^2)\cos[\alpha_1 - \alpha_2] = 0 \tag{10}$$

$$\frac{a_1}{2}(\omega_{n1}^2 - \omega_r^2)\sin[\alpha_1 - \alpha_2] = 0 \tag{11}$$

Here, Equations 8 and 10 are the real parts of the harmonic balance and 9 and 11 are the imaginary parts. From the imaginary parts, it can be seen that, for a non-trivial solution, it must be true that $\sin[\alpha_1 - \alpha_2] = 0$ and, hence, we must have either $\alpha_1 = \alpha_2$ or $\alpha_1 = \alpha_2 + \pi$, ignoring the possibility of adding 2π to either solution. At this stage, the notation $p = \cos[2(\alpha_1 - \alpha_2)]$ is introduced, following the lead of Hill et al. [3]. The authors demonstrated that $p = \pm 1$, where $p = 1$ corresponds to the case $|\alpha_1 - \alpha_2| = n\pi$ and $p = -1$ corresponds to the case $|\alpha_1 - \alpha_2| = \frac{(2n\pi - 1)}{2}$; an explanation for this is not given here for reasons of conciseness, but can be found in Appendix A of the paper. These equations can now be written in the form

First Mode:

$$\begin{aligned}\frac{a2}{2}(\omega_{n2}^2 - \omega_r^2 + \frac{3}{4}(3a_1^2\kappa_1 + a_2^2(\kappa 1 + 8\kappa 2)))\sqrt{\frac{1+p}{2}} \\ + \frac{a1}{2}((\omega_{n1}^2 - \omega_r^2 + \frac{3}{4}((a_1^2 + 2a_2^2) + a_2^2\kappa_1 p)) = 0\end{aligned} \tag{12}$$

$$-\frac{a2}{2}(\omega_{n2}^2 - \omega_r^2 + \frac{3}{4}(a_1^2\kappa_1 + a_2^2(\kappa 1 + 8\kappa 2) + 2a_1a_2\kappa_1\sqrt{\frac{1+p}{2}}))\sqrt{\frac{1-p}{2}} = 0 \tag{13}$$

Second Mode:

$$\frac{a2}{2}(\omega_r^2 - \omega_{n2}^2 - 6a_2^2\kappa_2) + \frac{a1}{2}(\omega_{n1}^2 - \omega_r^2)\sqrt{\frac{1+p}{2}} = 0 \tag{14}$$

$$\frac{a1}{2}(\omega_{n1}^2 - \omega_r^2)\sqrt{\frac{1-p}{2}} = 0 \tag{15}$$

Implementing these values for the phase, Equations 8 and 10 have been solved using Wolfram Alpha, with the results being discussed in Section 3.

2.2.2 Second-Order Normal Forms

This method consists of the linear modal, forcing, and nonlinear near-identity transforms to the physical equations of motion in Equation 3.

The first of these converts the equations of motion, Equation 3, from physical coordinates, $\mathbf{x}$, to modal coordinates, $\mathbf{q}$; this is shown in Section 2.1.

In the standard procedure for the second-order normal forms method, the forcing transfer, $\mathbf{q} \to \mathbf{v}$, is to be applied. However, since the system under consideration is unforced, this transform is just unity. That is, $\mathbf{v} = \mathbf{q}$.

Finally, the nonlinear near-identity transform is applied. This step separates the fundamental and harmonic components of v by introducing the substitution $\mathbf{v} = \mathbf{u} + \mathbf{h}$, with $\mathbf{u}$ and $\mathbf{h}$ representing the fundamental and harmonic parts of the response, respectively. A number of assumptions are made:

- As both the harmonics and the nonlinearities are small, $\mathbf{N}_v(\mathbf{v}) = \mathbf{N}_v(\mathbf{u})$; this is due to the fact that the second term in the Taylor expansion is a small variation of a small term.
- The fundamental response of each mode will be sinusoidal, meaning that, for the i^{th} mode

$$u_i = u_{ip} + u_{im} = \frac{U_i}{2}(e^{+j(\Omega t - \phi_i)} + e^{-j(\Omega t - \phi_i)}) \tag{16}$$

The application of this transform results in the resonant equation of motion:

$$\ddot{\mathbf{u}} + \mathbf{\Lambda u} + \mathbf{N_u}(\mathbf{u}) = \mathbf{0} \tag{17}$$

where $\mathbf{N_u}(\mathbf{u})$ is the matrix containing the elements of $\mathbf{N_v}(\mathbf{u})$ and 0 for the other entries. To find the resonant matrix, the matrices are written in the form

$$\mathbf{N_v} = \mathbf{n_v}\mathbf{u}^*, \;\; \mathbf{N_u} = \mathbf{n_u}\mathbf{u}^* \tag{18}$$

Here, $\mathbf{u}^*$ is a matrix of all the possible combination of u_{ip} and u_{im} in $\mathbf{N_v}(\mathbf{u})$ and $\mathbf{n_v}$ and $\mathbf{n_u}$ are matrices containing the coefficients of each of these combinations. The resonant terms in $\mathbf{u}^*$ are found using the matrix

$$\boldsymbol{\beta} = \left(\left[\sum_{k=1}^{2}\{s_{\ell kp} - s_{\ell kp}\}\right]^2 - 1\right)\Omega^2 \tag{19}$$

where $s_{\ell kp}$ and $s_{\ell kp}$ are defined by writing the ℓ^{th} term in $\mathbf{u}^*$ as

$$u_\ell^* = \prod_{k=1}^{2}\left\{u_{kp}^{s_{\ell kp}} u_{km}^{s_{\ell kp}}\right\} \tag{20}$$

Now, we may populate $\mathbf{n_u}$ via the following definition for element $\{i, \ell\}$, which arises due to the fact that a zero entry in the $\{i, \ell\}$ position of $\boldsymbol{\beta}$ corresponds to the coefficient of a resonant term:

$$n_{u,i\ell} = \begin{cases} n_{v,i\ell} & \text{if } \beta_{i\ell} = 0, \\ 0 & \text{otherwise.} \end{cases} \tag{21}$$

Therefore, the matrices $\mathbf{u}^*$, $\mathbf{n_v}$, $\boldsymbol{\beta}$ and, hence, $\mathbf{n_u}$ are given by

$$\mathbf{u}^* = \begin{bmatrix} u_{1p}^3 \\ u_{1p}^2 u_{1m} \\ u_{1p} u_{1m}^2 \\ u_{1m}^3 \\ u_{1p} u_{2p}^2 \\ u_{1p} u_{2p} u_{2m} \\ u_{1p} u_{2m}^2 \\ u_{1m} u_{2p}^2 \\ u_{1m} u_{2p} u_{2m} \\ u_{1m} u_{2m}^2 \\ u_{1p}^2 u_{2p} \\ u_{1p}^2 u_{2m} \\ u_{1p} u_{1m} u_{2p} \\ u_{1p} u_{1m} u_{2m} \\ u_{1m}^2 u_{2p} \\ u_{1m}^2 u_{2m} \\ u_{2p}^3 \\ u_{2p}^2 u_{2m} \\ u_{2p} u_{2m}^2 \\ u_{2m}^3 \end{bmatrix}, \mathbf{n}_\mathbf{v}^T = \begin{bmatrix} 1 & 1 \\ 3 & 3 \\ 3 & 3 \\ 1 & 1 \\ 3 & 3 \\ 6 & 6 \\ 3 & 3 \\ 3 & 3 \\ 6 & 6 \\ 3 & 3 \\ 3 & 3 \\ 3 & 3 \\ 6 & 6 \\ 6 & 6 \\ 3 & 3 \\ 3 & 3 \\ \alpha & 1 \\ 3\alpha & 3 \\ 3\alpha & 3 \\ \alpha & 1 \end{bmatrix}, \boldsymbol{\beta}^T = \begin{bmatrix} 8 & 8 \\ 0 & 0 \\ 0 & 0 \\ 8 & 8 \\ 8 & 8 \\ 0 & 0 \\ 0 & 0 \\ 0 & 0 \\ 0 & 0 \\ 8 & 8 \\ 8 & 8 \\ 0 & 0 \\ 0 & 0 \\ 0 & 0 \\ 0 & 0 \\ 8 & 8 \\ 8 & 8 \\ 0 & 0 \\ 0 & 0 \\ 8 & 8 \end{bmatrix}, \mathbf{n}_\mathbf{u}^T = \begin{bmatrix} 0 & 0 \\ 3 & 3 \\ 3 & 3 \\ 0 & 0 \\ 0 & 0 \\ 6 & 6 \\ 3 & 3 \\ 3 & 3 \\ 6 & 6 \\ 0 & 0 \\ 0 & 0 \\ 3 & 3 \\ 6 & 6 \\ 6 & 6 \\ 3 & 3 \\ 0 & 0 \\ 0 & 0 \\ 3\alpha & 3 \\ 3\alpha & 3 \\ 0 & 0 \end{bmatrix} \tag{22}$$

where $\alpha = 1 + 16\frac{\kappa 2}{\kappa 1}$.

From these matrices, $\mathbf{N_u}$ can be calculated and substituted into Equation 17; the resultant equations are omitted for reasons of brevity. However, it can be seen from Equation 16 that the coefficients of $e^{+j\Omega t}$ and $e^{-j\Omega t}$ in this equation are complex conjugates and, hence, must both be zero. This leads to the following equations

$$\begin{aligned} (\omega_{n1}^2 - \omega_r^2)U_1 + \frac{9\kappa_1}{8m}(U_1^3 + 3U_1U_2^2 + p(3U_1^2U_2 + \alpha U_2^3)) = 0 \\ (\omega_{n2}^2 - \omega_r^2)U_2 + \frac{9\kappa_1}{8m}(U_1^3 + 3U_1U_2^2 + p(3U_1^2U_2 + U_2^3)) = 0 \end{aligned} \tag{23}$$

where $p = \pm 1$, as before. Equations 23 have been solved using Wolfram Mathematica and the results are discussed in Section 3.

2.2.3 Multiple Scales

The Method of Multiple Scales (MMS) is a perturbation technique in which the dependent variable, q, is assumed to be separated into a series of increasingly small parts. Namely, this separation will take the form

$$q_i = q_{i0} + \varepsilon q_{i1} + \varepsilon^2 q_{i2} + ... + \varepsilon^n q_{in} + ... \tag{24}$$

Here, ε is a small bookkeeping term which ensures that the contribution of q_{ij} decreases as j increases. For this study, the perturbation will be truncated at the first order of ε, so $q_i = q_{i0} + \varepsilon q_{i1}$. In MMS, the derivatives of q_i are also perturbed, which requires a further perturbation of the time scale. These will again utilise ε to introduce a series of successively slower time-scales, denoted by

$$T_n = \varepsilon^n t \quad \text{for} \quad n = 1, 2, ... \tag{25}$$

Using these time-scales, and again truncating at the first order of ε, the derivatives become

$$\begin{aligned} \frac{d}{dt} &= D_0 + \varepsilon D_1 \\ \frac{d^2}{dt^2} &= D_0^2 + 2\varepsilon D_0 D_1 \end{aligned} \tag{26}$$

Here, D_i denotes differentiation with respect to T_i. This method will also be applied directly to the linear modal equations of motion given in Equation 5, with ε being introduced to denote the relatively small contribution of the nonlinear terms:

$$\ddot{\mathbf{q}} + \mathbf{\Lambda q} + \varepsilon \mathbf{N_q}(\mathbf{q}) = \mathbf{0} \tag{27}$$

It is first necessary to expand the equations of motion and collect the ε terms; only the first mode equation is shown here:

$$\begin{aligned} &2D_0^2 q_{10}(T_0) + 2\omega_{\mathrm{n}1}^2 q_{10}(T_0) + \varepsilon\Big(4D_0 D_1 q_{10}(T_0) + 2D_0^2 q_{11}(T_0) + \\ &\frac{\kappa_1 q_{10}(T_0)^3}{m} + \frac{3\kappa_1 q_{20}(T_0) q_{10}(T_0)^2}{m} + \frac{3\kappa_1 q_{20}(T_0)^2 q_{10}(T_0)}{m} + \frac{\kappa_1 q_{20}(T_0)^3}{m} + 2\omega_{\mathrm{n}1}^2 q_{11}(T_0)\Big) \;=\; 0 \end{aligned} \tag{28}$$

This results in the following zeroth-order perturbation equation

$$\begin{aligned} q_{10}(\omega_{n1}^2 - \omega_r^2) &= 0 \\ q_{20}(\omega_{n2}^2 - \omega_r^2) &= 0 \end{aligned} \tag{29}$$

Therefore, a modified version of the assumed sinusoidal response in Equation 7 is used in this method, with the phase and amplitude now considered as functions of the "slow" time-scale T_1. This allows the amplitude to be thought of as close to steady-state. Therefore, the solution is assumed to take the form

$$q_i = A_i(T_1)e^{+j\omega_r T_0} + \bar{A}_i(T_1)e^{-j\omega_r T_0} = \frac{a_i}{2}\Big(e^{+j(\omega_r T_0 + \alpha_i)} + e^{-j(\omega_r T_0 + \alpha_i)}\Big) \tag{30}$$

This solution can then be substituted into the first-order perturbation equation, though this is omitted due to its unwieldy nature. Thankfully, it is only necessary to consider the secular terms in this equation (that is, those terms including the term $e^{iT_0\omega_r}$). The sum of the secular terms must be zero to avoid solution divergence with time [9].

The system will also respond to frequencies in a small neighbourhood of the natural frequency. Hence, detuning parameters are introduced around ω_{ni}. For the i^{th} mode,

$$\omega_r = \omega_{ni} + \varepsilon\sigma_i \tag{31}$$

To aid the finding of steady-state solutions, the following linear transformations are applied to the phase angles, rendering the system autonomous.

$$\begin{aligned} \Psi_1(T_1) &= \sigma_1 T_1 - \alpha_1(T_1) \\ \Psi_2(T_1) &= \sigma_2 T_1 - \alpha_2(T_1) \end{aligned} \tag{32}$$

Then, steady-state solutions occur when

$$\begin{aligned} &a_i'(T_1) = 0 \\ &\Psi_i'(T_1) = 0 \implies \alpha_i'(T_1) = \sigma_i \end{aligned} \tag{33}$$

Implementing Equation 33 in the secular equation and separating the real and imaginary parts results in the following equations, respectively:

$$\begin{aligned}
&\frac{1}{8}\left(3a_2\kappa_1\left(a_1^2\cos\left(2\left(\alpha_1-\alpha_2\right)\right)+2a_1^2+a_2^2\right)+a_1\cos\left(\alpha_1-\alpha_2\right)\left(3a_1^2\kappa_1+9a_2^2\kappa_1-16\sigma_1\omega_r\right)\right)=0\\
&\frac{1}{8}a_1\sin\left(\alpha_1-\alpha_2\right)\left(6a_2a_1\kappa_1\cos\left(\alpha_1-\alpha_2\right)+3a_1^2\kappa_1+3a_2^2\kappa_1-16\sigma_1\omega_r\right)=0
\end{aligned} \tag{34}$$

Similar equations are found for the second mode; most importantly, the $\sin\left(\alpha_1-\alpha_2\right)$ term is also present in the imaginary equation, meaning that $\alpha_1=\alpha_2$ or $\alpha_1=\alpha_2+\pi$, as with the Harmonic Balance. Introducing the phase notation from [3] gives the following form for these equations:

$$\begin{aligned}
&\frac{1}{8}\left(3a_2\kappa_1\left((p+2)a_1^2+a_2^2\right)+a_1\sqrt{\frac{1+p}{2}}\left(3a_1^2\kappa_1+9a_2^2\kappa_1-16\sigma_1\omega_r\right)\right)=0\\
&\frac{1}{8}a_1\sqrt{\frac{1-p}{2}}\left(6a_2a_1\kappa_1\sqrt{\frac{1+p}{2}})+3a_1^2\kappa_1+3a_2^2\kappa_1-16\sigma_1\omega_r\right)=0
\end{aligned} \tag{35}$$

These equations have been solved using the former case and the results and discussion are provided in the next section.

2.3 Forced Response

Calculating the forced responses is a more complex process, due to the introduction of the damping and, in particular, forcing terms; the forcing terms introduce an explicit dependence on time, which is not present when solving for the backbone curves. Taking this into consideration, only the SONF and Harmonic Balance techniques were used for this section.

To allow the effects of forcing on the individual modes to be investigated, modal forcing will be implemented using the term:

$$\mathbf{P}=\begin{pmatrix}P_1\\P_2\end{pmatrix}\cos(\Omega t)$$

In Figure 1, P_{x1} and P_{x2} represent the resultant forcing on the physical displacement of the first and second masses, respectively. Hence, the linear forcing is defined using the modeshape matrix Φ as

$$\begin{pmatrix}P_{\mathrm{x1}}\\P_{\mathrm{x2}}\end{pmatrix}=2m\begin{pmatrix}P_1+P_2\\P_1-P_2\end{pmatrix}$$

The forcing on the two modes, and hence the two masses, is assumed to be at the same frequency, Ω. Applying the linear modal transformation to the physical equations of motion results in the following linear modal equations:

$$\ddot{\mathbf{q}}+\mathbf{\Lambda q}+\mathbf{N_q}(\mathbf{q},\dot{\mathbf{q}})=\mathbf{P}\cos(\Omega\mathrm{t}) \tag{36}$$

Here, $\mathbf{\Lambda}$ and $\mathbf{P}$ are as before and $\mathbf{N}_q$ now includes the damping terms:

$$\mathbf{N}_q(\mathbf{q},\dot{\mathbf{q}})=\begin{pmatrix}2\zeta_1\omega_{n1}\\2\zeta_2\omega_{n2}\end{pmatrix}\dot{\mathbf{q}}+\frac{\kappa_1}{2\mathrm{m}}\begin{pmatrix}(q_1+q_2)^3\\(q_1+q_2)^3+\alpha q_2^3\end{pmatrix} \tag{37}$$

The process of solving these equations is the same as in Section 2, so it is not repeated here, but the full equations are given in the following section, along with the plotted results and discussion.

3 Results and Discussion

3.1 Backbone Curves

Equations 8 - 11 have been solved to give the backbone curve equations for Harmonic Balance and the same has been done with Equation 34 for Multiple Scales. Simplifying these and doing the same for the Equation

23 allows a direct comparison between the results from each method. The solutions for each method are as follows:

Nonlinear Normal Forms:

$$\begin{aligned} &\frac{3\kappa_1(U_1+U_2)^3}{8m} + U_1(\omega_{n1}^2 - \omega_r^2) = 0 \\ &\frac{3(16\kappa_2 U_2^3 + \kappa_1(U_1+U_2)^3)}{8m} + U_2(\omega_{n2}^2 - \omega_r^2) = 0 \end{aligned} \tag{38}$$

Harmonic Balance:

$$\begin{aligned} &\frac{3\kappa_1(A_1+A_2)^3}{8m} + A_1(\omega_{\mathrm{n1}}^2 - \omega_r^2) = 0 \\ &\frac{3(16\kappa_2 A_2^3 + \kappa_1(A_1+A_2)^3)}{8m} + A_2(\omega_{n2}^2 - \omega_r^2) = 0 \end{aligned} \tag{39}$$

Multiple Scales:

$$\begin{aligned} &\frac{3\kappa_1(a_1+a_2)^3}{8m} + 2a_1(\omega_{n1}\omega_r - \omega_r^2) = 0 \\ &\frac{3(16\kappa_2 a_2^3 + \kappa_1(a_1+a_2)^3)}{8m} + 2a_2(\omega_{n2}\omega_r - \omega_r^2) = 0 \end{aligned} \tag{40}$$

It is immediately clear that these solutions are all very similar, particularly the SONF and Harmonic Balance solutions, which are identical after standardising the notation for amplitude. The second terms in the Multiple Scales equations are noticeably different to those from the two previously mentioned techniques, however, this is because this technique attempts to linearise the system, so the linear term of the Taylor expansions of $a_i(\omega_{ni}^2 - \omega_r^2)$ arises in this Equation 40. Hence, when the frequency detuning is large, the error in this approximation is significant.

These solutions are compared with the numerical results from *AUTO-07p* in the Figures 2 and 3. Firstly, these figures show that the approximations from all three techniques are very close to numerically derived results for the level of detuning considered. The main discrepancies between the numerical and analytical results arise due to the fact that the harmonics of the system are assumed to be negligible. For this system, these assumptions are clearly valid, though this may not hold true for more complicated systems. In this case, it is technically possible to include the superharmonics, though the practicality of this is discussed later.

Secondly, the effect that the Multiple Scales method's linearisation of the system has on the final results is evident. The solutions are still undoubtedly accurate, but they do not match the numerical solutions to the same extent as the other analytical methods. To this end, the error between the Multiple Scales and other methods has been approximated using the assumption $U_i \approx A_i \approx a_i$ as

$$A_i(\omega_{ni} - \omega_r)^2 \tag{41}$$

From this approximation, it is simple to deduce that the error will be greatest at higher amplitudes and at frequencies which are a greater distance from the structure's natural frequencies. Using this, the maximum error over the considered range has been calculated:

Table 1 indicates that, across the considered region, the error caused by the linearisation in the Multiple Scales method is never greater than 1%. The error is more apparent in the second mode, but the diverging behaviour suggested by the approximation in Equation 41 is apparent across all four backbone curves.

From this point forward, the analytical response discussed will only be that from the SONF and Harmonic Balance methods. As previously discussed, these are analytically identical, however, there is some

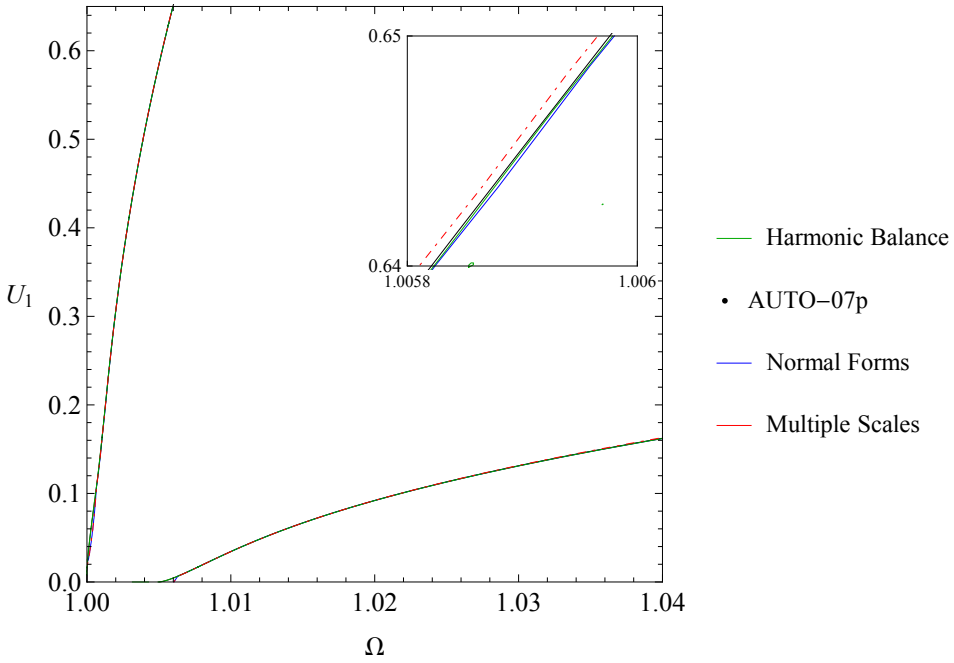

Figure 2: A comparison of the Harmonic Balance, Nonlinear Normal Forms, and Multiple Scales methods with numerical results from AUTO-07p in terms of q_1.

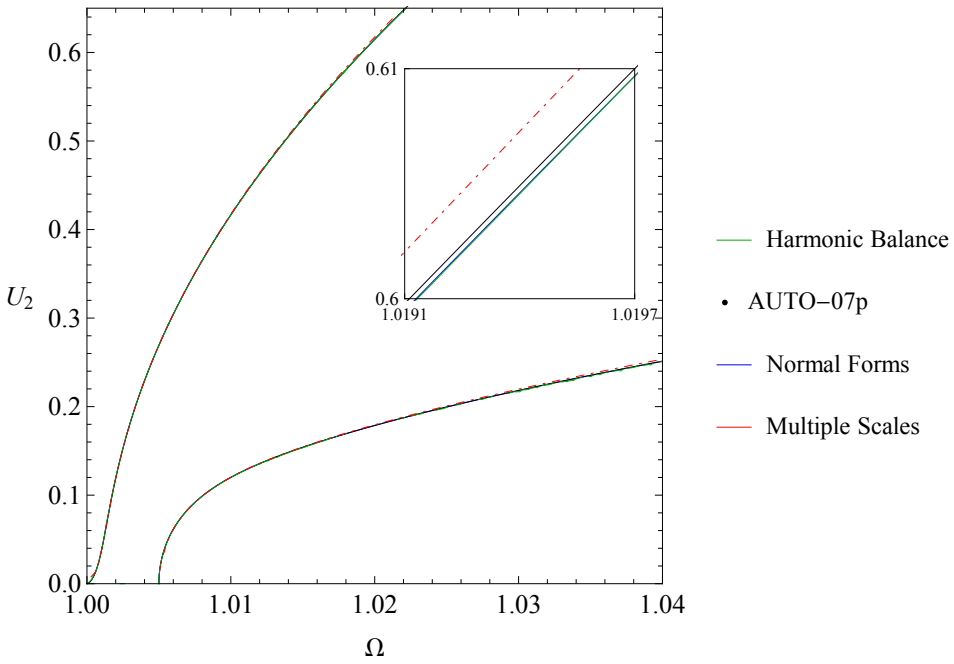

Figure 3: A comparison of the Harmonic Balance, Nonlinear Normal Forms, and Multiple Scales methods with numerical results from AUTO-07p in terms of q_2.

Table 1: Maximum percentage errors (%) between the Multiple Scales and Nonlinear Normal Forms/Harmonic Balance techniques, and between the approximation techniques and numerical continuation, in the calculation of the system's backbone curves over the considered region

	MMS		**Analytical**	
	A_1	A_2	A_1	A_2
First Mode	0.144	0.509	0.025	0.172
Second Mode	0.645	0.997	0.061	0.128

disagreement between the plotted curves. This is due to numerical differences in the implementation of these equations.

The analytical approximation errors in Table 1 are noticeably smaller than the Method of Multiple Scales errors and, in fact, they are never greater than 0.2%. This demonstrates the excellent level of accuracy achieved by the analytical approximations, even without consideration of the superharmonics. As previously mentioned, this is unlikely to be the case for some systems, though the investigation of this is beyond the scope of this study.

3.2 Forced Responses

The techniques and methodology of solving the forced equations of motion were identical to those for the backbone curves and so they are not repeated here. However, the following equations have been found for the forced responses of the system:

Nonlinear Normal Forms:

$$\begin{aligned}
&\frac{3\kappa_1(U_1+U_2)^3}{16m}+\frac{U_1}{2}(\omega_{n1}^2-\Omega^2)-\frac{\sqrt{(P_1+4mU_1\omega_{n1}\Omega\zeta)(P_1-4mU_1\omega_{n1}\Omega\zeta)}}{4m}=0\\
&\frac{3(\kappa_1(U_1+U_2)^3+16U_2^3)}{16m}+\frac{U_2}{2}(\omega_{n2}^2-\Omega^2)-\frac{\sqrt{(P_2+4mU_2\omega_{n2}\Omega\zeta)(P_2-4mU_2\omega_{n2}\Omega\zeta)}}{4m}=0
\end{aligned} \tag{42}$$

Harmonic Balance:

$$\begin{aligned}
&\frac{3\kappa_1(A_1+A_2)^3}{16m}+\frac{A_1}{2}(\omega_{n1}^2-\Omega^2)-\frac{\sqrt{(P_1+4mA_1\omega_{n1}\Omega\zeta)(P_1-4mA_1\omega_{n1}\Omega\zeta)}}{4m}=0\\
&\frac{3(\kappa_1(A_1+A_2)^3+16A_2^3)}{16m}+\frac{A_2}{2}(\omega_{n2}^2-\Omega^2)-\frac{\sqrt{(P_2+4mA_2\omega_{n2}\Omega\zeta)(P_2-4mA_2\omega_{n2}\Omega\zeta)}}{4m}=0
\end{aligned} \tag{43}$$

The two sets of equations are identical, as they were for the backbone curves. This result is somewhat expected, as it is the same system being considered, however, it is important to note that the introduction of the explicitly time-dependent forcing term does not affect this outcome.
The forced responses for the analytical solution and numerical continuation have been plotted for the following three cases:

Table 2: Magnitudes of forcing for the three considered cases

	P_1	P_2
First Mode Forcing	0.0015	0
Second Mode Forcing	0	0.0015
Mixed Mode Forcing	0.0015	0.0015

The damping coefficient is set at $\zeta = 0.004$ and all other variables will take the same value as in the unforced, undamped case. Implementing these values results in the following graphs; these will only be displayed in the first modal coordinate, though the accuracy is the same for both.
A different approach had to be taken for the plotting of these curves, namely, an ad hoc continuation method was used. The reason for this is that the response phases, ϕ_1 and ϕ_2, now have a physical meaning. In the unforced case, the two variables were used to represent the difference in phase between the two modes, whereas they now represent the difference in phase between the two modes relative to the forcing frequency, Ω. This technique entailed finding an initial linear approximation for $\Omega = 0.96$, then incrementally increasing Ω and using the previous values of U_1, U_2, ϕ_1, ϕ_2 as an initial approximation for the current step. It is clear from Figures 4, 5, and 6 that this method is extremely accurate; the two lines are practically indistinguishable, even in the more complicated mixed mode case.

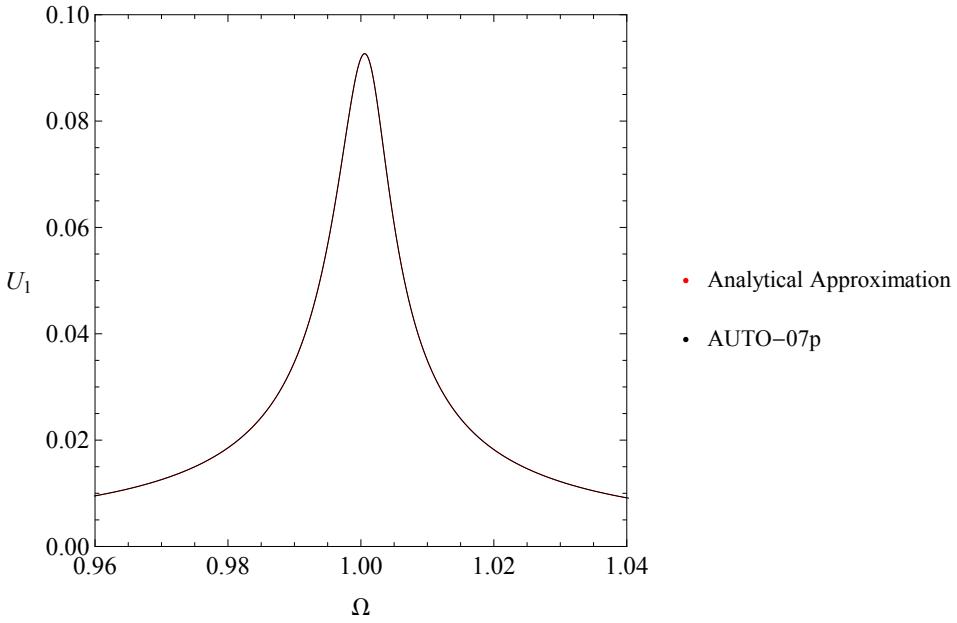

Figure 4: A comparison of the first mode forced response calculated by analytical approcimation methods with numerical results from AUTO-07p in terms of q_1.

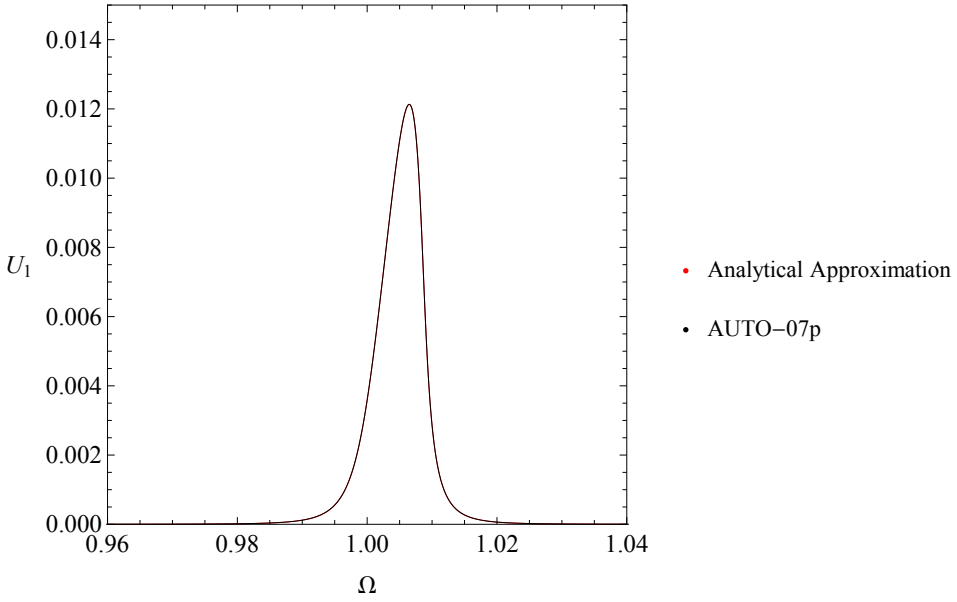

Figure 5: A comparison of the second mode forced response calculated by analytical approcimation methods with numerical results from AUTO-07p in terms of q_1.

To more clearly illustrate the difference between the analytical techniques and the numerical continuation results, Figure 7 displays a closer view of the peak in the first mode forcing case. Since the two curves are generated by continuation, at this enlarged view, the curve is seen to be a series of straight lines between the calculated points. Therefore, it is much more difficult to give the maximum error. However, it is noticeable that the two lines actually intersect at many of the calculated points, even at the highest amplitude, suggesting a high level of accuracy from the analytical approximation.

4 Conclusions

In this paper, a comparison has been made between the accuracy and practicality of applying the Second-Order Normal Forms, Harmonic Balance, and Multiple Scales methods to a non-symmetric, nonlinear two-mass oscillator. These techniques were first applied to the unforced, undamped structure to find the systems

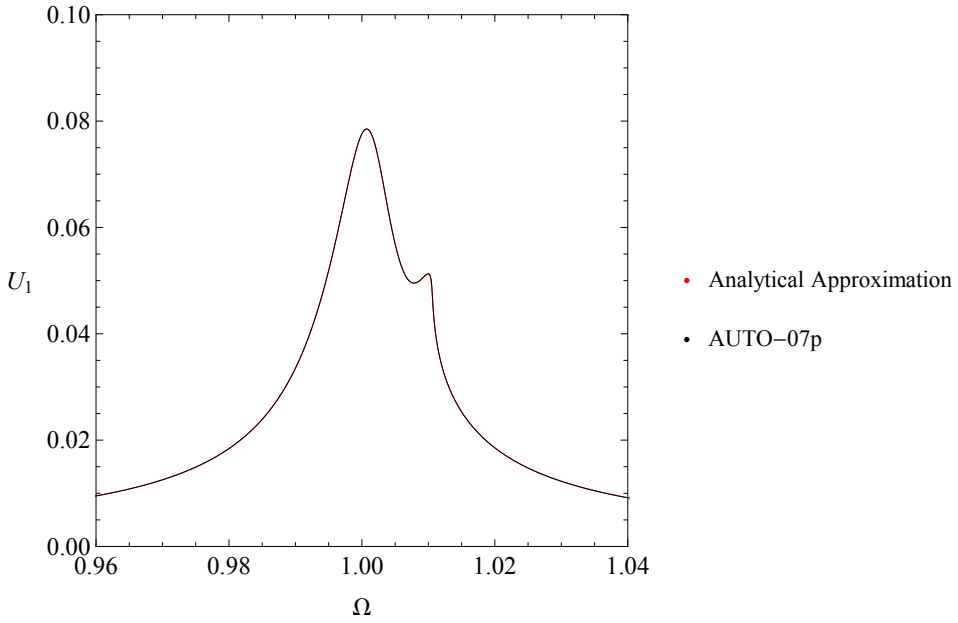

Figure 6: A comparison of the mixed mode forced response calculated by analytical approcimation methods with numerical results from AUTO-07p in terms of q_1.

backbone curves. An interesting outcome of the study is that, for this case, the analytical solutions from the SONF and Harmonic Balance method were identical; furthermore, the only difference between this solution and the Multiple Scales solution was that one of the terms has been replaced by the linear term of its Taylor expansion. All three methods were seen to give an accurate representation of this curve, with the error not being greater than 0.2% for the SONF and Harmonic Balance methods, and 1% for the Multiple Scales method.

The difference between these methods therefore arises in the practicality of their application. The Multiple Scales method was found to be the least workable, as evidenced by the fact that the zeroth order perturbation for the forced case was not feasibly solvable. The introduction of additional time-scales also added extra steps that complicated the procedure. The two remaining techniques both arrived at the same solution, though the Harmonic Balance method does so in less steps. This would suggest that the Harmonic Balance is the more practical method to use, however, the plotting of the graphs (both using the ContourPlot feature in *Wolfram Mathematica*) proved to be less time-consuming for the SONF method.

Although these results could suggest an advantage in using the Harmonic Balance, this may not be the case for more complex systems. A key difference in the efficiency of the Harmonic Balance and SONF techniques was encountered when attempting to calculate the harmonic vibrations of the system. The SONF method's matrix framework allows these to be included with little additional calculation necessary and little added computational cost added. However, it is very difficult to replicate this using the Harmonic Balance; for instance, the simultaneous equations including the third harmonic quickly became too complex to solve reasonably, even with the use of *Wolfram Mathematica*. It is likely that the Harmonic Balance would not be able to reach the same level of accuracy as the SONF method in systems in which the harmonics play a greater role in the structure's dynamics.

References

[1] S.A. Neild, A.R. Champneys, D.J. Wagg, T.L. Hill, and A. Cammarano. The use of normal forms for analysing nonlinear mechanical vibrations. *Philosophical Transactions of the Royal Society A*, 373(2051), 2015.

[2] A. Cammarano, T.L. Hill, S.A. Neild, and D.J. Wagg. Bifurcations of backbone curves for systems of coupled nonlinear two mass oscillators. *Nonlinear Dynamics*, 77:311–320, 2014.

[3] T.L. Hill, A. Cammarano, S.A. Neild, and D.J. Wagg. Interpreting the forced responses of a two-degree-

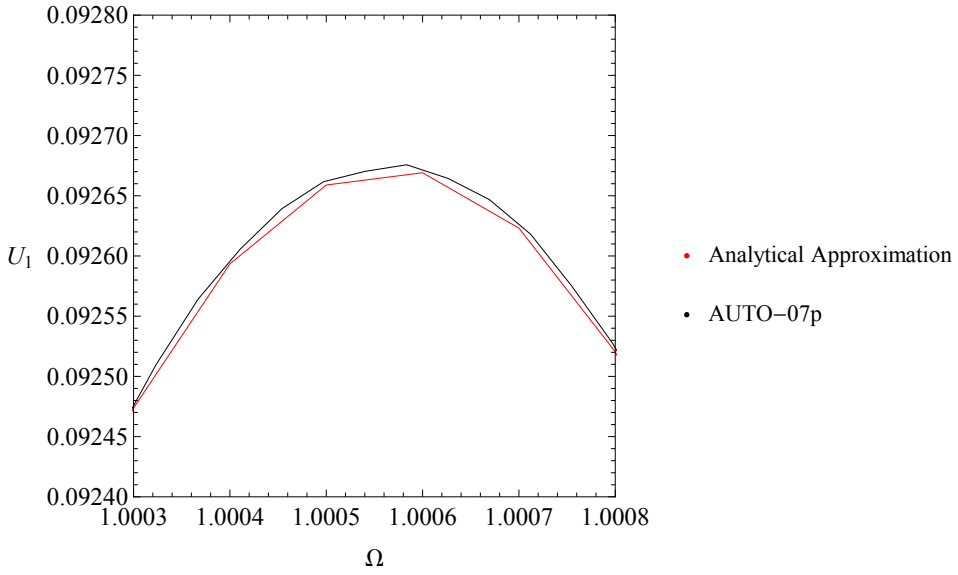

Figure 7: An enlarged view of the turning point in Figure 4.

of-freedom nonlinear oscillator using backbone curves. *Journal of Sound and Vibration*, 349:276–288, 2015.

[4] S. Neild and D.J. Wagg. Applying the method of normal forms to second-order nonlinear vibration problems. *Proceedings of the Royal Society A*, 467:1141–1163, 2011.

[5] A.H. Nayfeh. *The Method of Normal Forms*. Wiley-VCH, 2011.

[6] X. Liu, A. Cammarano, D.J. Wagg, S.A. Neild, and R.J. Barthorpe. N-1 modal interactions of a three-degree-of-freedom system with cubic elastic nonlinearities. *Nonlinear Dynamics*, 83(1):497–511, 2016.

[7] T.L. Hill, A. Cammarano, S.A. Neild, and D.J. Wagg. Relating backbone curves to the forced responses of nonlinear systems. In G. Kerschen, editor, *Proceedings of the 33rd IMAC, A Conference and Exposition on Structural Dynamics*, volume 1, pages 113–122, 2015.

[8] E.J. Doedel, A.R. Champneys, T.F. Fairgrieve, Y.A. Kuznetsov, F. Dercole, B.E. Oldeman, R.C. Paffenroth, B. Sandstede, X.J. Wang, and C. Zhang. Auto-07p: Continuation and bifurcation software for ordinary differential equations, Montreal, Concordia University, Canada, 2008.

[9] D. Wagg and S. Neild. *Nonlinear Vibration with Control: For Flexible and Adaptive Structures*. Springer, second edition, 2015.